minerals

MDPI

Article

Age and Geochemistry of Zircon Megacrysts from Alluvial Deposits in the Huadian Area, Northeastern China

Haiqi Sun [1], Shaokui Pan [1,2,*], Hongyu Qin [3], Yimiao Liu [1] and Xiaolong Wu [1]

[1] Gemological Institute, China University of Geosciences, Wuhan 430074, China
[2] Hubei Gems and Jewelry Engineering Technology Research Center, Wuhan 430074, China
[3] School of Prospecting and Surveying Engineering, Changchun Institute of Technology, Changchun 130012, China
* Correspondence: skpan@cug.edu.cn

Abstract: Megacrystic zircons have recently been found in alluvial deposits in the Huadian area of northeastern China. However, studies have rarely been conducted on these zircons. In this article, we present systematic in situ trace element, U-Pb age and Hf isotope data regarding these Huadian zircons, with the aim of investigating their source characteristics and provenance. The studied zircons, with a diameter of 0.7–1.2 cm, are dominantly irregular in shape and have a rounded termination, with a color ranging from near-colorless to reddish brown to maroon. The zircons show oscillatory zoning in CL images, with a Th/U value of 0.18–1.27, which is consistent with the typical features of magmatic zircons. The positive $\varepsilon_{Hf}(t)$ value of Huadian zircons (4.8–9.2) further indicates the presence of precipitation from the mantle-derived melt, with limited contamination of the crustal components. The obtained weighted mean $^{206}Pb/^{238}U$ age for these zircons is 17.9 ± 0.12 Ma, which is slightly older than the eruptional ages of the associated alkali basalts (from 17.6 ± 1.09 Ma to 17.8 ± 0.69 Ma), implying a short residence time in the mantle before entrainment. Huadian zircons incorporate a wide range of trace elements, including ΣREE (117–2790 ppm), Hf (4902–11856 ppm) and Y (145–3645 ppm) contents, generating mixed-source protolith assignments. As is suggested by the moderate variations seen in the Hf isotopes, we propose that the source melts of Huadian zircons are complex in nature, which is likely the result of the chemical heterogeneity of the upper mantle.

Keywords: zircon megacrysts; Huadian; U-Pb age; Hf isotope; trace element composition

check for updates

Citation: Sun, H.; Pan, S.; Qin, H.; Liu, Y.; Wu, X. Age and Geochemistry of Zircon Megacrysts from Alluvial Deposits in the Huadian Area, Northeastern China. *Minerals* **2023**, *13*, 882. https://doi.org/10.3390/min13070882

Academic Editor: Yamirka Rojas-Agramonte

Received: 23 April 2023
Revised: 15 June 2023
Accepted: 20 June 2023
Published: 29 June 2023

Copyright: © 2023 by the authors. Licensee MDPI, Basel, Switzerland. This article is an open access article distributed under the terms and conditions of the Creative Commons Attribution (CC BY) license (https://creativecommons.org/licenses/by/4.0/).

1. Introduction

Zircon ($ZrSiO_4$) is a ubiquitous accessory mineral that can be found in many types of terrestrial and extraterrestrial rocks [1,2]. It acts as a carrier for a wide range of elements, including REEs, Th, U, Hf, Pb and Ti. More importantly, zircon is chemically resistant and presents high closure temperatures and low diffusion rates for these elements as well as their isotopes, ensuring its widespread use for dating rock formations and constraining source protolith and crystallization conditions [3–5].

Megacrystic zircons (which are typically centimeter-sized) are found within intraplate alkali basalt deposits around the world; their derivatives are formed as a result of secondary processes, especially those seen in the countries along the western Pacific continental margins [6–9]. These basalts commonly contain abundant mantle xenoliths, along with a variety of high-pressure megacrysts such as corundum, pyroxene, garnet and spinel [10–13], offering scientists an opportunity to elucidate the composition and evolutionary history of the deep lithosphere. Some species of megacrysts (e.g., corundum and zircon) have also been commercially exploited for several centuries to supply the global market with gemstones [14]. Based on the Hf and O isotopic data, most previous studies argue that the zircon megacrysts associated with alkali basalts have a mantle affinity [15–20]. However, the nature of the source melt in the context of these large-sized zircons and their relationship with their host volcanic rocks are still a matter of fierce debate.

Eastern China is characterized by the widespread occurrence of Cenozoic basalts, with a spatial coverage of over 2500 km [21]. The basalts are mainly composed of alkali basalts, with a minor contribution made by tholeiites. Zircon megacrysts have been reported in several locations in eastern China, including Muling, Changle, Mingxi and Penglai, moving from north to south (Figure 1a). Zircon megacrysts from these locations are variable in terms of U-Pb ages (1–20 Ma) but have a predominantly positive $\varepsilon_{Hf}(t)$ value falling between the depleted mantle and chondrite values, implying precipitation from mantle-derived melts with limited involvement of older components [22,23]. Recently, an assemblage of megacrysts (corundum, zircon, pyroxene and garnet) were found in the alluvial deposits seen along the Huifa River in the Huadian area, Jilin province, northeastern China (Figure 1a). Corundum can also be termed sapphire, due to its blue coloration. Some corundum megacrysts are of gemstone quality and have thus been selected for further cutting into faceted stones. In contrast, little attention has been paid to other types of megacrysts, hampering our understanding of their source characteristics. In turn, tracing the source characteristics of these megacrysts is undoubtedly helpful for further explorations of these gemstone resources. Therefore, this study presents systematic in situ trace element, U-Pb age and Hf isotope data regarding the zircon megacrysts found in the Huadian area, with the aim of investigating their age, crystallization period and provenance.

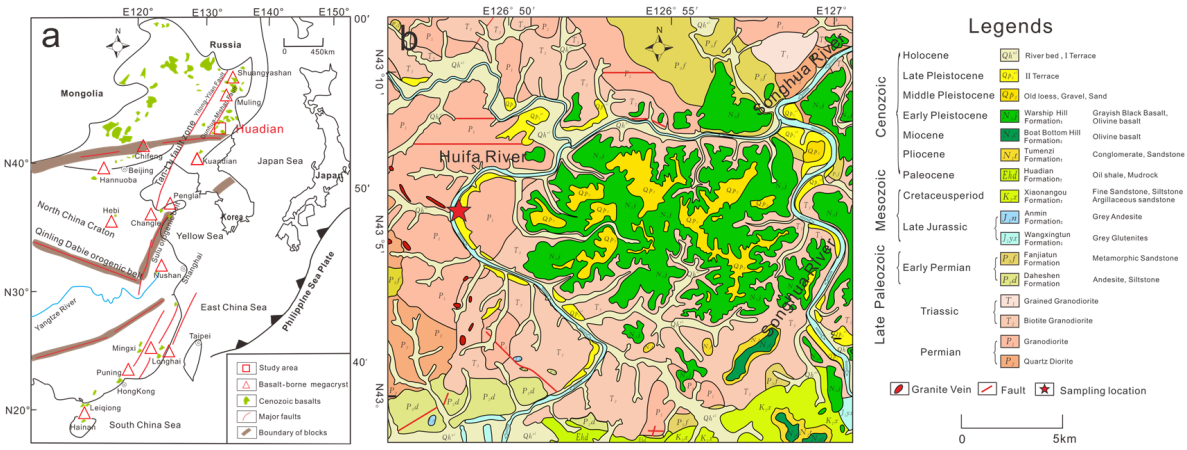


Figure 1. (**a**) A sketch map of eastern China showing the distribution of the Cenozoic basalts that contain megacrysts (modified from a previous work [11]); (**b**) a geological map of the studied area (modified from a previous work [24]).

2. Geological Background and Sample Description

Geological Background

Tectonically speaking, northeastern China belongs to the eastern segment of the Central Asian Orogenic Belt, which lies between the North China Craton to the south and the Siberia Craton to the north [25,26]. In some reference works, most parts of northeastern China are also called Manchuria [27]. During the Phanerozoic era, this fold belt was controlled by the Paleo-Asian Ocean tectonic regime and was characterized by the amalgamation of different tectonic components, such as ophiolites, island arcs, oceanic islands, accretion complexes and Precambrian microcontinents [28–32]. Although a theory that is still controversial, it is widely accepted that the Paleo-Asian Ocean finally closed in the late Permian or middle Triassic period [28,33,34]. Since early Mesozoic times, northeastern China has been strongly influenced by circum-Pacific tectonic events and the closure of the Mongol-Okhotsk Ocean, accompanied by the occurrence of voluminous granitoids and minor intermediate-felsic volcanic rocks [34,35]. Subsequently, this large area entered a period of magmatic cessation until the eruption of the Cenozoic basalts [36,37].

The city of Huadian is located near the Dunhua–Mishan fault zone (Figure 1a), which is considered to be the northern branch of the well-known Tanlu translithospheric fault zone [38,39]. The studied area is dominated by Triassic granitoids and Permian volcanic and sedimentary rocks. Cenozoic basalts are mainly found in the area between two local watercourses, the Huifa and Songhua rivers (Figure 1b). These basalts are predominantly alkali olivine basalts, with K-Ar ages ranging from 17.6 ± 1.09 Ma to 17.8 ± 0.69 Ma [40]. All the zircon samples in this study were collected from the alluvial deposits on the concave bank of the Huifa River.

3. Methods

A backscatter image photography experiment was conducted by the Nanjing Hongchuang Geological Exploration Technology Service Co., Ltd. (Nanjing, China). The emission scanning electron microscope used for the experiment was the TESCAN Mira3 LMH, while the BSE probe was supplied by the company TESCAN. The samples were coated with conductive film before imaging. The operating voltage was set at 20 kV for the backscatter test. The backscatter probe was moved at a low multiple while in field mode to identify the sample. Focus (WD) and astigmatism (STG) were adjusted repeatedly until the image was clear and showed appropriate brightness and contrast levels.

Cathodoluminescence (CL) imaging was also performed on resin targets to observe the internal structure of the zircons at the Nanjing Hongchuang Geological Exploration Technology Service Co., Ltd. The resin target was cleaned using an ultrasonic wave and was then coated with carbon before analysis. The CL images were obtained using a Tescan MIRA3 LM instrument equipped with a CL detector. The applied acceleration voltage and current were set at consistent values of 7 kV. Each CL image was collected in an 80 s accumulation and shared an overlapping area of about 15% with the surrounding images to ensure the seamless stitching of the panorama.

In situ U-Pb dating and trace element analysis of the zircon were simultaneously conducted using LA-ICP-MS at the Wuhan SampleSolution Analytical Technology Co., Ltd., Wuhan, China. Detailed operating conditions for the laser ablation system and the ICP-MS instrument and data reduction are the same as those described by the authors of [41]. Laser sampling was performed using a GeolasPro laser ablation system, consisting of a COMPexPro 102 ArF excimer laser (with a wavelength of 193 nm and a maximum pulse energy of 200 mJ) and a MicroLas optical system. An Agilent 7900 ICP-MS instrument was used to acquire the ion signal intensities. Helium was employed as a carrier gas, while argon was used as the makeup gas and was mixed with the carrier gas via a T-connector before entering the ICP. The spot size and frequency of the laser were set to 32 μm and 5 Hz, respectively. Zircon 91,500 and glass NIST610 were used as the external standards for U-Pb dating and trace element calibration, respectively. Each analysis incorporated a background acquisition of approximately 20–30 s, followed by 50 s of data acquisition from the sample itself. ICPMSDataCal was used to perform the off-line selection and integration of the background and analyzed signals, time-drift correction and quantitative calibration for the purposes of trace element analysis and U-Pb dating [42,43]. Concordia diagrams and weighted mean calculations were made using Isoplot/Ex_ver3 [44].

Analyses of the in situ Hf isotope ratio were conducted using a Neptune Plus MC-ICP-MS (Thermo Fisher Scientific, Bremen, Germany) in combination with a Geolas HD excimer ArF laser ablation system (Coherent, Göttingen, Germany) located at the Wuhan Sample Solution Analytical Technology Co., Ltd. A "wire" signal smoothing device is included in this laser ablation system, meaning that smooth signals are produced, even at very low laser repetition rates of 1 Hz [45]. Helium was used as the carrier gas within the ablation cell and was merged with argon (makeup gas) beyond the ablation cell. Small amounts of nitrogen were added to the argon makeup gas flow to improve the sensitivity of the Hf isotopes [46]. Compared to the standard arrangement, the addition of nitrogen, in combination with the use of the newly designed X skimmer cone and Jet sample cone in the Neptune Plus, improved the signal intensity of Hf, Yb and Lu by a factor of 5.3, 4.0 and

2.4, respectively. All data were acquired on zircon using the single-spot ablation mode at a spot size of 44 µm. The energy density of the laser ablation employed in this study was set at ~7.0 J cm^{-2}. Each measurement consisted of 20 s of acquisition of the background signal, followed by 50 s of ablation signal acquisition. Detailed operating conditions for the laser ablation system and the MC-ICP-MS instrument and the analytical method are the same as those described by the authors of [46].

4. Results

4.1. Zircon Morphology and Internal Structure

Sixteen zircon grains, with a diameter of 0.7–1.2 cm, were selected for observation of the internal structure and further geochemical experiments. Their color varied from near-colorless to reddish brown to maroon (Figure 2). Zircon grains are mainly irregular in shape, with a rounded termination. The primary crystal planes are difficult to identify. After double-polishing (at a thickness of about 0.4 cm), some zircons showed internal colored zones that were marked by an oscillatory change of near-colorless and reddish-brown bands visible to the naked eye. The patterns of the internal colored zones were roughly comparable to those seen in cathodoluminescence (CL) images.



Figure 2. Appearance characteristics of representative zircons sourced from Huadian.

Twelve zircon megacrysts clearly showed magmatic oscillatory growth zoning without the presence of a relict core (Figure 3a–c). The width of the oscillatory growth area varied significantly, ranging from several microns to more than thirty microns. Although still identifiable, oscillatory zoning was faint in four samples (for example, HD-9; Figure 3d). Local sector zoning patches could occasionally be observed in several samples in which oscillatory zoning dominated (Figure 3a). Two samples (HD-1 and HD-4), although showing oscillatory growth zoning, were composed of two parts that visibly differed in brightness (Figure 3e,f). They presented indistinguishable $^{206}Pb/^{238}U$ ages and $\varepsilon_{Hf}(t)$ values but showed different trace element compositions, such as those for Th and U (see Section 4.3).

4.2. U-Pb Geochronology and Hf Isotopic Compositions

The results of the U-Pb dating and Hf isotope analysis of the zircon megacrysts from Huadian are listed in Tables S1 and S2, respectively, in the Supplementary Materials. Five to eight analytical spots of U-Pb dating were conducted per grain of zircon (from one rim to the other, via the core). Most of the U-Pb dating results are concordant, assuming a concordance of >90% (100(1 − abs($^{206}Pb/^{238}U$ age − $^{207}Pb/^{235}U$ age)/(($^{206}Pb/^{238}U$ age + $^{207}Pb/^{235}U$ age)/2))). However, the ages of $^{207}Pb/^{235}U$ are relatively imprecise because of the low abundance of radiogenic ^{207}Pb and the relatively small size of the selected laser spot. In contrast, the $^{206}Pb/^{238}U$ ages are more robust; therefore, they can be used for analysis. The studied zircons lacked significant differences in the ages of $^{206}Pb/^{238}U$ between the core and the rim of each zircon (Figure 3). The absence of detected inherited cores is consistent with the lack of an obvious core structure in the CL images. These zircons also demonstrated weighted mean $^{206}Pb/^{238}U$ ages indistinguishable from each other (17.1 ± 1.0~18.6 ± 1.1 Ma; see Table S1 in the Supplementary Materials), implying that they were formed during a single-stage growth event. All analyses of the zircons

from Huadian yielded a weighted mean $^{206}Pb/^{238}U$ age of 17.9 ± 0.12 Ma (MSWD = 1.3; Figure 4).

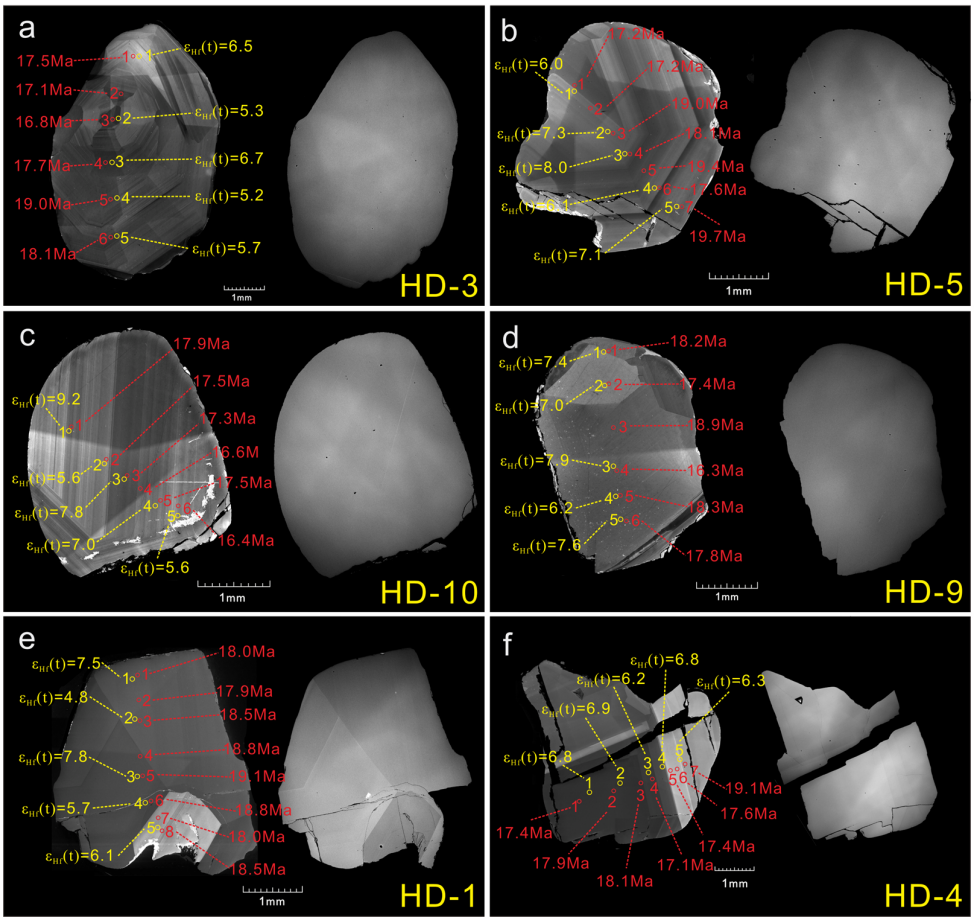


Figure 3. Representative CL and backscattered images of the zircon megacrysts from Huadian: obvious oscillatory zoning is shown in samples HD-5 (**b**) and HD-10 (**c**), while faint oscillatory zoning is shown in sample HD-9 (**d**) and local sector zoning is shown in sample HD-3 (**a**). Growth zoning consists of two areas of different brightness, as seen in samples HD-1 (**e**) and HD-4 (**f**). Red circles mark the locations of U-Pb analysis, while yellow circles mark the locations of Hf isotope analysis.

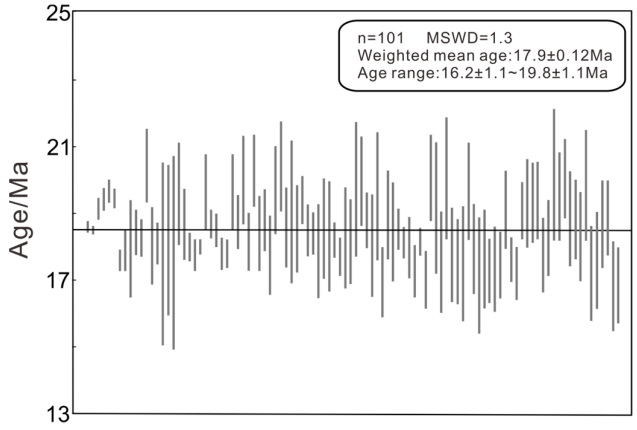


Figure 4. The weighted average $^{206}Pb/^{238}U$ age of the Huadian zircons.

Five Hf isotope analyses were carried out on each zircon grain. Although there were slight variations in $^{176}Hf/^{177}Hf$ within each grain, no systematic differences in $^{176}Hf/^{177}Hf$ between the core and rim were observed. Generally, all analyses showed a moderate

range of $^{176}Hf/^{177}Hf$, from 0.282898 ± 22 to 0.283020 ± 22 (1SE). Correspondingly, the $\varepsilon_{Hf}(t)$ values of the studied zircons ranged from 4.8 to 9.2 (Figure 5) when the obtained weighted mean $^{206}Pb/^{238}U$ age of 17.9 ± 0.12 Ma was adopted. The T_{DM} and $T_{crustal}$ model ages of the zircon megacrysts from Huadian varied from 324 Ma to 560 Ma and from 513 Ma to 791 Ma, respectively. Yu et al. (2010) [23] suggested that the $\varepsilon_{Hf}(t)$ values of the zircon megacrysts found in eastern China decrease southward (from Changle via Mingxi to Penglai; see Figure 1a). However, such a trend disappears with the inclusion of the zircon megacrysts from Muling and Huadian (Figure 5).

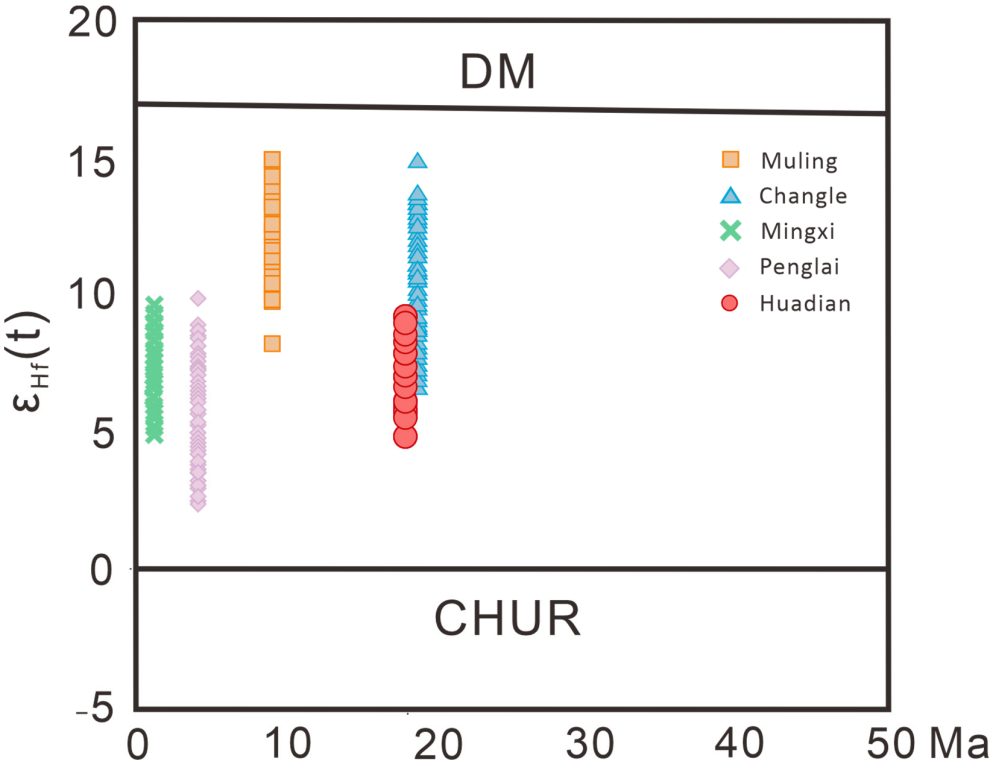


Figure 5. Diagram of the $\varepsilon_{Hf}(t)$ values vs. U-Pb ages. Data on the zircon megacrysts from Muling, Changle, MingXi and Penglai are drawn from previous studies [23,47].

4.3. Trace Element Compositions

The trace element composition of zircon megacrysts from Huadian is shown in Table S3 in the Supplementary Materials. All zircons were depleted of LREE and enriched in HREE, with clearly positive Ce anomalies in the chondrite-normalized REE patterns (Figure 6). No negative Eu anomalies can be observed, except in the case of sample HD-1, which shows a slightly negative Eu anomaly. Most zircon megacrysts (except for samples HD-1 and HD-4) have a Th/U value of 0.30–0.79, with low ΣREE contents of below 500 ppm. Relative to the bright part of the sample, the dark part of sample HD-1 is clearly higher in Th (2155 ppm vs. 362 ppm), U (1692 ppm vs. 741 ppm), Nb (31 ppm vs. 6.70 ppm) and Th/U (1.27 vs. 0.49). This characteristic also applies to sample HD-4. The dark part of HD-4 is higher in Th (813 ppm vs. 23.58 ppm), U (811 ppm vs. 134 ppm), Nb (24.65 ppm vs. 3.72 ppm) and Th/U (1.00 vs. 0.18) than the bright part of the sample. The dark part of HD-4 also contains higher Ta (14.73 ppm vs. 7.053 ppm) and ΣREE (1016 ppm vs. 295 ppm) contents than the bright part of the sample. The Ti content in the zircons is low (less than 3 ppm, except in the case of HD-2, which has a Ti content of 7.91 ppm).

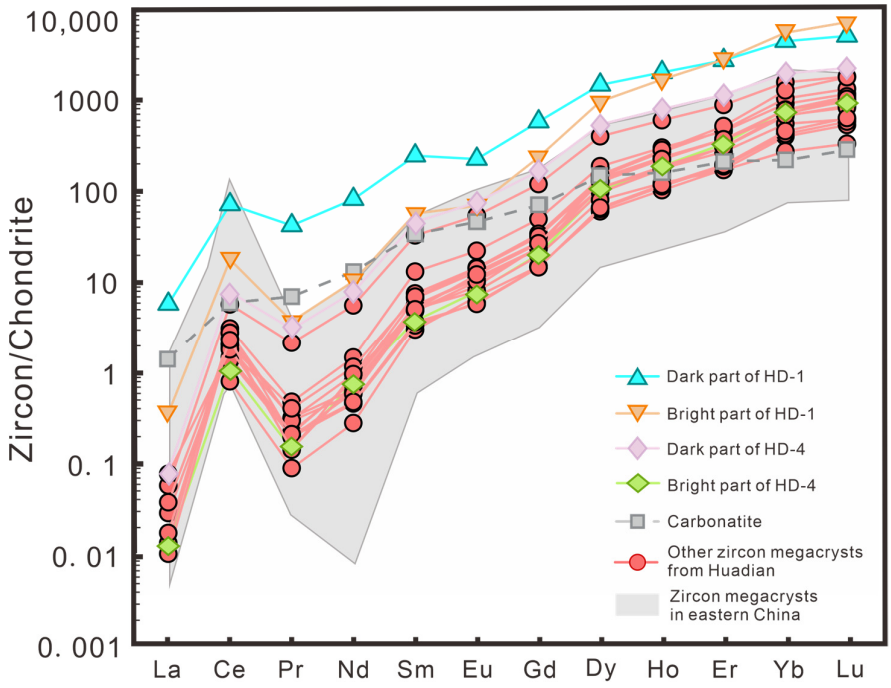


Figure 6. Chondrite-normalized REE pattern for the zircon megacrysts from Huadian. The normalization values of chondrite are from a previous study [48]. The chondrite-normalized averaged REE patterns of zircons established from granitoid, carbonatite and kimberlite are from a previous study [3]. The data used for the zircon megacrysts from eastern China are the same as those in Figure 5.

5. Discussion

5.1. Source Affinities of Zircon Megacrysts

Because the zircon megacrysts studied in this paper were collected from placer deposits along the local river, where they have been separated from the host rocks, it is necessary to investigate their source affinities before further discussion can take place. All the zircons from Huadian showed oscillatory zoning in the CL images, which is generally considered to be a typical feature of magmatic zircons [49,50]. They have relatively high Th/U values, varying from 0.18 to 1.27, which is generally consistent with the range of Th/U recorded for igneous zircons (0.2–1.0) [4]. The studied zircons have Lu values of > 10 ppm (except for HD-12, which had a Lu value of 8.70 ppm) and $(Lu/Dy)_N > 3.93$, implying that they are not in equilibrium with a substantial garnet (Zhu et al., 2022) [51]. Huadian zircons do not exhibit a pronounced negative Eu anomaly (Figure 6), which is commonly observed in zircons taken from crustal-derived rocks; Eu^{2+} would be concentrated into plagioclase, which crystallizes before or during zircon precipitation from the parental melt [4,52]. This is consistent with the absence of feldspar megacrysts in the studied area. More importantly, the studied zircons have positive $\varepsilon_{Hf}(t)$ values ranging from 4.8 to 9.2, seen for those from the juvenile depleted mantle and those from the chondrite reservoir (Figure 5), indicating that they crystallized from a mantle-derived melt without significant crustal contamination. The zircon megacrysts from Huadian have ΣREE contents that range from 117 ppm to 2790 ppm (mostly below 500 ppm), which is generally comparable with those of zircons associated with alkali basalts worldwide [3]. In addition, the assemblage of megacrysts from Huadian (corundum, zircon, garnet and pyroxene) is quite similar to those eroded from host basalts during the formation of paleo/present placers from various locations in eastern China, as well as those found in other countries along the western Pacific continental margins, such as Cambodia, Thailand, Australia and Vietnam [7,8,22,23]. The widespread occurrence of the Cenozoic alkali basalts in the studied area and nearby regions (Figure 1) also increases the likelihood of such a possibility.

5.2. Age Relationship between Zircon Megacrysts and Host Basalts

Attention must be paid when interpreting the U-Pb age of megacrystic zircons that are associated with mantle-derived volcanic rocks, because the high temperature of the host magma may reset the U-Pb isotope systems found in zircons. If this is true, the U-Pb isotopic results for zircons likely record the eruptional ages of their host rocks instead of the formational ages of the zircons. However, many studies have revealed that the crystallization ages of mantle-derived zircons are clearly older than the eruptions of transporting kimberlitic or basaltic magmas [18,53–56], implying that zircons could retain their formational ages under high-temperature conditions (for example, those in the upper mantle and lower crust). Most of the U-Pb dating results for the zircon megacrysts from Huadian are concordant, without significant Pb-loss. Therefore, the complete resetting of the U-Pb isotope systems in the studied zircons appears to be impossible. We interpreted this to mean that the U-Pb age of the zircons, as obtained in this study, represents their crystallization ages.

Recent geochronological studies suggest that the Cenozoic alkali basalts in the Huadian area have K-Ar ages ranging from 17.6 ± 1.09 Ma to 17.8 ± 0.69 Ma [40]. Although the K-Ar method presents some uncertainties in terms of dating volcanic rocks, such as the gaining of K as a result of alteration, from the available data, it seems that the studied zircons (with a weighted mean $^{206}Pb/^{238}U$ age of 17.9 ± 0.12 Ma) formed slightly earlier than the eruption of their host basalts. This finding is in agreement with the well-developed oscillatory zoning of zircons from Huadian as a long period of residence under high-temperature conditions could blur the growth zoning of zircons [1]. Such a near-coeval relationship between the zircon megacrysts and their host basalts has also been identified in samples from other locations (Penglai, Changle and Mingxi) throughout eastern China, reflecting the rapid ascent of these zircons shortly after formation, as suggested by the authors of [23]. It appears unrealistic that zircons can directly crystallize from basaltic magmas because a very high Zr content is required for mafic melts (more than 5000 ppm [57]). Therefore, the occurrence of zircon megacrysts from Huadian (and other locations from eastern China) reveals the presence of unerupted Zr-saturated parental melts in the deep lithosphere beneath the Huadian area (and even in eastern China). However, recent experimental studies argue that zircon could form and survive dissolution in the deep lithosphere or asthenosphere under specific conditions involving fluids and intercumulus melts or fluids [58]. Therefore, whether the studied zircons are cognate with their host alkali basalts needs further investigation. Considering the widespread occurrence of zircon megacrysts in eastern China and the western Pacific continental margins, we consider that these basalts likely served only as the host rocks that carried the zircon megacrysts to the surface.

5.3. Provenance of Zircon Megacrysts

Several origins have been proposed for the formation of the zircon megacrysts associated with intraplate alkali basalts, including (1) crystallization from a melt derived from the metasomatized mantle [7,15,59]; (2) formation during a late-stage fractional process of OIB [53]; (3) crystallization from a primitive alkaline mafic magma, which subsequently evolved into a less alkaline magma [16]. All arguments agree upon the mantle's affinity with the zircon megacrysts associated with alkali basalts. This is consistent with the positive $\varepsilon_{Hf}(t)$ value of the zircons from Huadian. Huadian zircons are variable in terms of ΣREE contents, ranging from 117 to 2790 ppm. However, they have U-Pb ages indistinguishable from each other, making it unlikely that they are products formed by the protracted fractional crystallization process of an evolving melt. Additionally, although there are moderate variations in some trace element concentrations, such as those of ΣREE, Th, U and Y, no systematic variations in these elements from core to rim can be observed, which is inconsistent with the continuous crystallization of zircon from a melt and evolution via fractional crystallization [4,16]. In addition, the absence of a significant Eu anomaly does not support the formation of zircons at a late stage in OIB magmatic differentiation. This is consistent with the absence of feldspar megacrysts in the studied area. Thus, it appears

more likely that the zircon megacrysts from Huadian were formed from a melt derived from the metasomatic mantle.

Trace element composition is helpful for defining the nature of the parental melt of igneous zircons in secondary placers [3,60]. Huadian zircons are chemically aligned to the values for continental crust rather than the oceanic crust values (Figure 7), which are commonly observed in zircon megacrysts from mantle-derived volcanic rocks such as kimberlites and carbonatites (Grimes et al., 2007) [61]. Most of the zircons from Huadian have a ΣREE content below 500 ppm. They also contain low Hf and Y levels that can be plotted in or adjacent to the carbonatite field (Figure 8). This finding also applies to zircon megacrysts from other locations in eastern China. However, strict discrimination of the type of source rock of igneous zircon, based on trace element composition, becomes less reliable with the involvement of additional datasets [4]. For example, several studies have revealed that the zircons found in carbonatites have a wide compositional variation and can fall into other fields, such as alkaline and ultramafic–intermediate rock fields [62,63]. Moreover, this does not mean that zircons with a carbonatitic signature are necessarily derived from carbonatitic rocks. In fact, exposed carbonatite seems absent in the studied area, to the best of the authors' knowledge. According to the experimental studies performed by Foley et al. (2009) [64], the upper mantle rocks metasomatized by volatile components (CO_2 and H_2O) have a lower solidus temperature. The partial melting of metasomatized peridotites would produce melts with carbonatitic compositions at a low degree, and carbonated silicate melts with further melting. Some recent studies have invoked such a model (partial melting of a carbonatitic-metasomatized mantle to a variable degree) to illustrate the generation of 'carbonatitic signature' zircon megacrysts, which are associated with alkali basalts found in Vietnam and Cambodia [10,14].

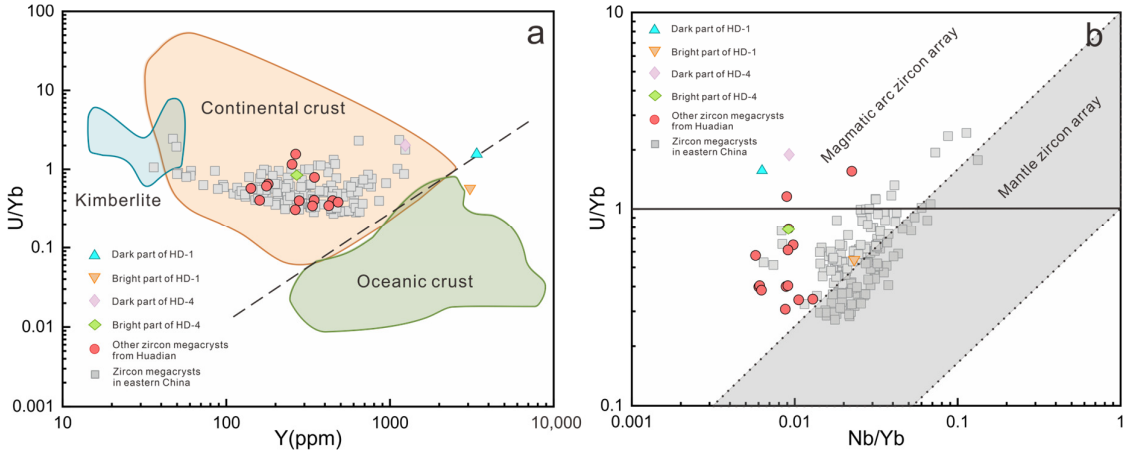


Figure 7. Y vs. U/Yb (**a**) and Nb/Yb vs. U/Yb (**b**). Data for the zircon megacrysts from eastern China are the same as those in Figure 5. Fields for the continental and oceanic crusts and kimberlite are according to Grimes et al. [61]. Fields for the mantle and magmatic arc arrays are according to Grimes et al. [65].

However, it appears difficult to simply reconcile the formation of zircon megacrysts from Huadian with crystallization from melts produced by the partial melting of a carbonatitic-influenced mantle to a variable degree. For example, the dark part of sample HD-1, with a Hf value of 5820 ppm, has a high ΣREE content of up to 2790 ppm. It contains a high Y of 3645 ppm, falling into the field of felsic rocks with high SiO_2 (Figure 8). Turner et al. (2020) [66] compiled a large dataset of whole-rock SiO_2 contents from the GEOROC database and suggested that the Th/Y of zircons show a robust positive correlation with the SiO_2 found in their source melt. According to the method followed by Turner et al. [66], the dark part of sample HD-1, with a Th/Y value of 0.59, requires a parental melt with a SiO_2 value of up to 70.9 wt %. In the same way, the dark part of sample HD-4, with a Th/Y value of 0.64, corresponds to a parental melt with a SiO_2 value of 72.6 wt %. The sample

has Hf and Y contents of 10,037 and 1275 ppm, respectively, placing it in the ultramafic–basic–intermediate rocks group (Figure 8). Silica-rich (SiO_2 > 60 wt %) melt inclusions were also identified in the zircon megacrysts from Penglai [22]. The generation of felsic parental melt does not necessarily require an evolving process, but it does likely reflect the local occurrence of Si-rich melt, which is considered to be an important metasomatic agent of the lithospheric mantle beneath eastern China [67,68]. On the other hand, if zircons gradually precipitate from a melt, their plots should follow an evolving trend rather than evincing a scatter distribution, as shown in Figure 8. Considering the indistinguishable ages of U-Pb contents, we interpret the wide range of trace element compositions found in Huadian zircons (as well as the moderate differences in Hf isotopes among the zircons) as reflecting the complexity of their source melts. This is further supported by the compositionally different domains (i.e., the dark part and bright part) of HD-1 and HD-4, which reflect a growth environment for the zircons that changed spontaneously into an environment with low Th and U contents (as well as other elements, such as Nb). Numerous studies on mantle xenoliths from eastern China have offered evidence that the subcontinental lithospheric mantle beneath eastern China is highly heterogeneous, even on a regional scale [69–73]. For example, petrological and geochemical studies on peridotite xenoliths from nearby Jiaohe (about 50 km away from Huadian) have revealed that the lithospheric mantle beneath that area experienced pervasive metasomatic processes that were caused by volatile-bearing silicate melts, showing a large range of $^{176}Hf/^{177}Hf$ from 0.282767 to 0.284588 [74,75]. Tectonic activities since the Mesozoic time, such as the upwelling of asthenospheric material and the subduction of oceanic plates (e.g., the western Pacific plate), may play a key role in the formation of a chemically heterogeneous upper mantle beneath eastern China [76–79].

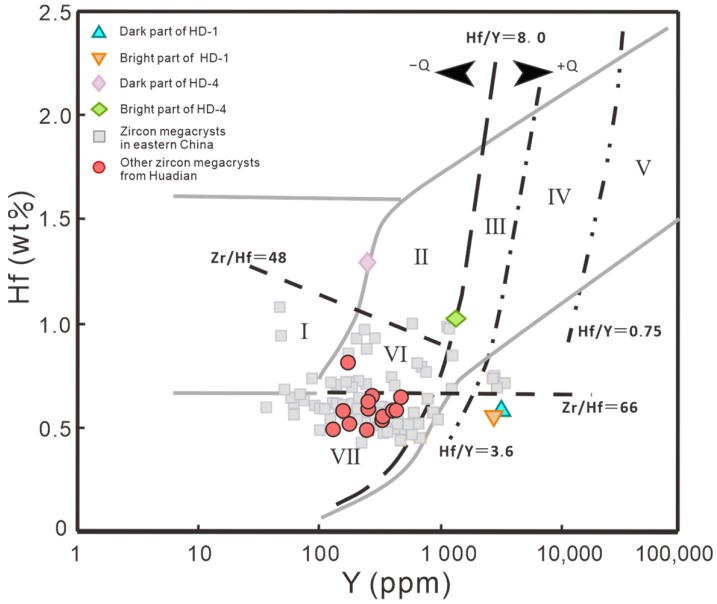


Figure 8. Discrimination diagram of Hf vs. Y, modified from a previous study [3]. (I) kimberlites; (II) ultramafic, mafic and intermediate rocks; (III) quartz-bearing intermediate and felsic rocks; (IV) felsic rocks with a high SiO_2 content; (V) greisens; (VI) alkaline rocks and alkaline metasomatites of the alkaline complexes; (VII) carbonatites. Data for the zircon megacrysts found in eastern China are the same as those shown in Figure 5.

6. Conclusions

(1) The zircon megacrysts from Huadian display oscillatory growth zoning in CL images. They have Th/U values of 0.18–1.27 and positive $\varepsilon_{Hf}(t)$ values from 4.8 to 9.2, indicating precipitation from a mantle-derived melt, with limited crustal contamination.

(2) The studied zircons have indistinguishable U-Pb ages (a weighted mean $^{206}Pb/^{238}U$ age of 17.9 ± 0.12 Ma), implying that they formed during a single-stage growth event. The coeval relationship between the zircons and the local alkali basalts suggests a very short mantle residence time for the zircons before entrainment.

(3) The wide range of trace element compositions of the zircons from Huadian, combined with their moderate variations in terms of Hf isotopes, reflects the complexity of their source magmas, which may be ascribed to the chemical heterogeneity of the upper mantle.

Supplementary Materials: The following supporting information can be downloaded at: https://www.mdpi.com/article/10.3390/min13070882/s1, Table S1: LA-ICP-MS U-Pb isotopic analyses of the studied zircon megacrysts; Table S2: Lu-Hf isotope composition of the studied zircon megacrysts; Table S3: Trace element (ppm) composition of the studied zircon megacrysts.

Author Contributions: Conceptualization, H.S. and S.P.; writing, H.Q.; review and editing, S.P.; supervision, H.Q.; investigation, Y.L. and X.W. All authors have read and agreed to the published version of the manuscript.

Funding: This research was funded by the National Natural Science Foundation of China, Grant No:41973032, 41530319.

Data Availability Statement: Not applicable.

Acknowledgments: We thank the journal editor and three anonymous reviewers for their constructive comments and suggestions. This research was also partly supported by the Gemological Institute, China University of Geosciences (CUG).

Conflicts of Interest: The authors declare no conflict of interest.

References

1. Corfu, F.; Hanchar, J.M.; Hoskin, P.W.O.; Kinny, P. Atlas of Zircon Textures. *Rev. Mineral. Geochem.* **2003**, *53*, 469–500. [CrossRef]
2. Valley, J.W.; Cavosie, A.J.; Ushikubo, T.; Reinhard, D.A.; Lawrence, D.F.; Larson, D.J.; Clifton, P.H.; Kelly, T.F.; Wilde, S.A.; Moser, D.E.; et al. Hadean Age for a Post-Magma-Ocean Zircon Confirmed by Atom-Probe Tomography. *Nat. Geosci.* **2014**, *7*, 219–223. [CrossRef]
3. Belousova, E.; Griffin, W.; O'Reilly, S.Y.; Fisher, N. Igneous Zircon: Trace Element Composition as an Indicator of Source Rock Type. *Contrib. Miner. Pet.* **2002**, *143*, 602–622. [CrossRef]
4. Hoskin, P.W.O.; Schaltegger, U. The Composition of Zircon and Igneous and Metamorphic Petrogenesis. *Rev. Mineral. Geochem.* **2003**, *53*, 27–62. [CrossRef]
5. Page, F.Z.; Fu, B.; Kita, N.T.; Fournelle, J.; Spicuzza, M.J.; Schulze, D.J.; Viljoen, F.; Basei, M.A.S.; Valley, J.W. Zircons from Kimberlite: New Insights from Oxygen Isotopes, Trace Elements, and Ti in Zircon Thermometry. *Geochim. Cosmochim. Acta* **2007**, *71*, 3887–3903. [CrossRef]
6. Graham, I.; Sutherland, L.; Zaw, K.; Nechaev, V.; Khanchuk, A. Advances in Our Understanding of the Gem Corundum Deposits of the West Pacific Continental Margins Intraplate Basaltic Fields. *Ore Geol. Rev.* **2008**, *34*, 200–215. [CrossRef]
7. Sutherland, F.L.; Duroc-Danner, J.M.; Meffre, S. Age and Origin of Gem Corundum and Zircon Megacrysts from the Mercaderes–Rio Mayo Area, South-West Colombia, South America. *Ore Geol. Rev.* **2008**, *34*, 155–168. [CrossRef]
8. Sutherland, L.; Graham, I.; Yaxley, G.; Armstrong, R.; Giuliani, G.; Hoskin, P.; Nechaev, V.; Woodhead, J. Major Zircon Megacryst Suites of the Indo-Pacific Lithospheric Margin (ZIP) and Their Petrogenetic and Regional Implications. *Min. Pet.* **2016**, *110*, 399–420. [CrossRef]
9. Abduriyim, A.; Sutherland, F.L.; Belousova, E.A. U–Pb Age and Origin of Gem Zircon from the New England Sapphire Fields, New South Wales, Australia. *Aust. J. Earth Sci.* **2012**, *59*, 1067–1081. [CrossRef]
10. Sinh, V.B.T.; Osanai, Y.; Lenz, C.; Nakano, N.; Adachi, T.; Belousova, E.; Kitano, I. Gem-Quality Zircon Megacrysts from Placer Deposits in the Central Highlands, Vietnam—Potential Source and Links to Cenozoic Alkali Basalts. *Minerals* **2019**, *9*, 89. [CrossRef]
11. Yu, X.; Zeng, G.; Chen, L.-H.; Hu, S.-L.; Yu, Z.-Q. Magma–Magma Interaction in the Mantle Recorded by Megacrysts from Cenozoic Basalts in Eastern China. *Int. Geol. Rev.* **2019**, *61*, 675–691. [CrossRef]
12. Sun, P.; Niu, Y.; Guo, P.; Duan, M.; Wang, X.; Gong, H.; Xiao, Y. The Lithospheric Thickness Control on the Compositional Variation of Continental Intraplate Basalts: A Demonstration Using the Cenozoic Basalts and Clinopyroxene Megacrysts from Eastern China. *J. Geophys. Res. Solid Earth* **2020**, *125*. [CrossRef]
13. Hu, L.; Pan, S.; Lu, R.; Zheng, J.; Dai, H.; Guo, A.; Yu, L.; Sun, H. Origin of Gem-Quality Megacrysts in the Cenozoic Alkali Basalts from the Muling Area, Northeastern China. *Lithos* **2022**, *422–423*, 106720. [CrossRef]

14. Piilonen, P.; Sutherland, F.; Danišík, M.; Poirier, G.; Valley, J.; Rowe, R. Zircon Xenocrysts from Cenozoic Alkaline Basalts of the Ratanakiri Volcanic Province (Cambodia), Southeast Asia—Trace Element Geochemistry, O-Hf Isotopic Composition, U-Pb and (U-Th)/He Geochronology—Revelations into the Underlying Lithospheric Mantle. *Minerals* **2018**, *8*, 556. [CrossRef]
15. Upton, B.G.J.; Hinton, R.W.; Aspen, P.; Finch, A.; Valley, J.W. Megacrysts and Associated Xenoliths: Evidence for Migration of Geochemically Enriched Melts in the Upper Mantle beneath Scotland. *J. Petrol.* **1999**, *40*, 935–956. [CrossRef]
16. Visonà, D.; Caironi, V.; Carraro, A.; Dallai, L.; Fioretti, A.M.; Fanning, M. Zircon Megacrysts from Basalts of the Venetian Volcanic Province (NE Italy): U–Pb Ages, Oxygen Isotopes and REE Data. *Lithos* **2007**, *94*, 168–180. [CrossRef]
17. Li, X.H.; Long, W.G.; Guo, C.H.; Liu, Y. Penglai Zircon: A Potential New Reference for Microbeam Analysis of U-Pb Age and O-Hf Isotopes. *Geochim. et Cosmochim. Acta* **2008**, *72*, A547. (In Chinese with English Abstract)
18. Siebel, W.; Schmitt, A.K.; Danišík, M.; Chen, F.; Meier, S.; Weiß, S.; Eroğlu, S. Prolonged Mantle Residence of Zircon Xenocrysts from the Western Eger Rift. *Nat. Geosci.* **2009**, *2*, 886–890. [CrossRef]
19. Simonetti, A.; Neal, C.R. In-Situ Chemical, U–Pb Dating, and Hf Isotope Investigation of Megacrystic Zircons, Malaita (Solomon Islands): Evidence for Multi-Stage Alkaline Magmatic Activity beneath the Ontong Java Plateau. *Earth Planet. Sci. Lett.* **2010**, *295*, 251–261. [CrossRef]
20. Schmitt, A.K.; Klitzke, M.; Gerdes, A.; Schäfer, C. Zircon Hafnium—Oxygen Isotope and Trace Element Petrochronology of Intraplate Volcanic Rocks from the Eifel (Germany) and Implications for Mantle versus Crustal Origins of Zircon Megacrysts. *J. Petrol.* **2017**, *58*, 1841–1870. [CrossRef]
21. Liu, R.X. *Chronology and Geochemistry of Cenozoic Volcanic Rocks in China*; Seismological Press: Beijing, China, 1992; ISBN 7-5028-0624-5.
22. Qiu, Z.; Wu, F.; Yu, Q.; Xie, L.; Yang, S. Hf Isotopes of Zircon Megacrysts from the Cenozoic Basalts in Eastern China. *Chin. Sci. Bull.* **2005**, *50*, 2602. [CrossRef]
23. Yu, Y.; Xu, X.; Chen, X. Genesis of Zircon Megacrysts in Cenozoic Alkali Basalts and the Heterogeneity of Subcontinental Lithospheric Mantle, Eastern China. *Min. Pet.* **2010**, *100*, 75–94. [CrossRef]
24. Jin, D.G. *Jilin City, Jilin Province, K-52-1 Regional Geological Survey Report, 1:200,000*; Jilin Provincial Bureau of Geology: Jilin, China, 1970.
25. Jahn, B.M.; Wu, F.; Chen, B. Granitoids of the Central Asian Orogenic Belt and Continental Growth in the Phanerozoic. *Spec. Pap. Geol. Soc. Am.* **2000**, *350*, 181–193. [CrossRef]
26. Windley, B.F.; Alexeiev, D.; Xiao, W.; Kröner, A.; Badarch, G. Tectonic Models for Accretion of the Central Asian Orogenic Belt. *JGS* **2007**, *164*, 31–47. [CrossRef]
27. Şengör, A.M.C.; Natal'in, B.A.; Burtman, V.S. Evolution of the Altaid Tectonic Collage and Palaeozoic Crustal Growth in Eurasia. *Nature* **1993**, *364*, 299–307. [CrossRef]
28. Xiao, W.; Windley, B.F.; Hao, J.; Zhai, M. Accretion Leading to Collision and the Permian Solonker Suture, Inner Mongolia, China: Termination of the Central Asian Orogenic Belt: Solonker Suturing in Inner Mongolia. *Tectonics* **2003**, *22*, 1–20. [CrossRef]
29. Zhou, J.-B.; Wilde, S.A.; Zhang, X.-Z.; Ren, S.-M.; Zheng, C.-Q. Early Paleozoic Metamorphic Rocks of the Erguna Block in the Great Xing'an Range, NE China: Evidence for the Timing of Magmatic and Metamorphic Events and Their Tectonic Implications. *Tectonophysics* **2011**, *499*, 105–117. [CrossRef]
30. Zhou, J.-B.; Li, L. The Mesozoic Accretionary Complex in Northeast China: Evidence for the Accretion History of Paleo-Pacific Subduction. *J. Asian Earth Sci.* **2017**, *145*, 91–100. [CrossRef]
31. Li, Y.; Xu, W.-L.; Zhu, R.-X.; Wang, F.; Ge, W.-C.; Sorokin, A.A. Late Jurassic to Early Early Cretaceous Tectonic Nature on the NE Asian Continental Margin: Constraints from Mesozoic Accretionary Complexes. *Earth-Sci. Rev.* **2020**, *200*, 103042. [CrossRef]
32. Şengör, A.M.C.; Lom, N.; Polat, A. The Nature and Origin of Cratons Constrained by Their Surface Geology. *GSA Bull.* **2022**, *134*, 1485–1505. [CrossRef]
33. Wu, F.-Y.; Zhao, G.-C.; Sun, D.-Y.; Wilde, S.A.; Yang, J.-H. The Hulan Group: Its Role in the Evolution of the Central Asian Orogenic Belt of NE China. *J. Asian Earth Sci.* **2007**, *30*, 542–556. [CrossRef]
34. Wang, C.; Jianchao, L.; Haidong, Z.; Jiakun, G.; Zhixuan, X.; Haoran, W. Mineralogical Features and Petrogenetic Significance of the Clinopyroxene and Hornblende of the Wuhaolai Mafic Complex in Northern North China Craton, Inner Mongolia. *Earth Sci. Res. J.* **2019**, *23*, 133–146. [CrossRef]
35. Tang, Y.J.; Zhang, H.F.; Ying, J.F. Genetic Significance of Triassic Alkali-Rich Intrusive Rocks in the Yinshan and Neighboring Areas. *Acta Petrol. Sin.* **2014**, *30*, 2031–2040. (In Chinese with English Abstract)
36. Zhang, M.; Suddaby, P.; O'Reilly, S.Y.; Norman, M.; Qiu, J. Nature of the Lithospheric Mantle beneath the Eastern Part of the Central Asian Fold Belt: Mantle Xenolith Evidence. *Tectonophysics* **2000**, *328*, 131–156. [CrossRef]
37. Pan, S.; Zheng, J.; Griffin, W.L.; Xu, Y.; Li, X. Nature and Evolution of the Lithospheric Mantle beneath the Eastern Central Asian Orogenic Belt: Constraints from Peridotite Xenoliths in the Central Part of the Great Xing'an Range, NE China. *Lithos* **2015**, *238*, 52–63. [CrossRef]
38. Sun, X.M.; Zhang, X.Q.; He, S.; Wang, P.J.; Zheng, H. Two Important Cretaceous Deformation Events of the Dunhua-Mishan Fault Zone. *Acta Petrol. Sin.* **2016**, *32*, 1114–1128. (In Chinese with English Abstract)
39. Zhu, G.; Liu, C.; Gu, C.; Zhang, S.; Li, Y.J. Oceanic Plate Subduction History in the Western Pacific Ocean: Constraint from Late Mesozoic Evolution of the Tan-Lu Fault Zone. *Sci. China Earth Sci.* **2018**, *61*, 386–405. [CrossRef]

40. JIN, K.; Guan, H.; Yu, M.; Yin, S.; GUO, Z.; Jia, H.; Chu, X.; Ren, J.; Wang, X. Prospecting Direction for Ruby and Sapphire from Cenozoic Basalt in Jilin Province. *Glob. Geol.* **2014**, *33*, 609–614. [CrossRef]
41. Zong, K.; Klemd, R.; Yuan, Y.; He, Z.; Guo, J.; Shi, X.; Liu, Y.; Hu, Z.; Zhang, Z. The Assembly of Rodinia: The Correlation of Early Neoproterozoic (ca. 900 Ma) High-Grade Metamorphism and Continental Arc Formation in the Southern Beishan Orogen, Southern Central Asian Orogenic Belt (CAOB). *Precambrian Res.* **2017**, *290*, 32–48. [CrossRef]
42. Liu, Y.; Hu, Z.; Gao, S.; Günther, D.; Xu, J.; Gao, C.; Chen, H. In Situ Analysis of Major and Trace Elements of Anhydrous Minerals by LA-ICP-MS without Applying an Internal Standard. *Chem. Geol.* **2008**, *257*, 34–43. [CrossRef]
43. Liu, Y.; Gao, S.; Hu, Z.; Gao, C.; Zong, K.; Wang, D. Continental and Oceanic Crust Recycling-Induced Melt-Peridotite Interactions in the Trans-North China Orogen: U-Pb Dating, Hf Isotopes and Trace Elements in Zircons from Mantle Xenoliths. *J. Petrol.* **2010**, *51*, 537–571. [CrossRef]
44. Ludwig, K.R. User's Manual for Isoplot/Ex Rev. 3.00: A Geochronological Toolkit for Microsoft Excel. *Berkeley Geochronol. Cent. Spec. Publ.* **2003**, *4*, 74.
45. Hu, Z.; Zhang, W.; Liu, Y.; Gao, S.; Li, M.; Zong, K.; Chen, H.; Hu, S. "Wave" Signal-Smoothing and Mercury-Removing Device for Laser Ablation Quadrupole and Multiple Collector ICPMS Analysis: Application to Lead Isotope Analysis. *Anal. Chem.* **2015**, *87*, 1152–1157. [CrossRef] [PubMed]
46. Hu, Z.; Liu, Y.; Gao, S.; Liu, W.; Zhang, W.; Tong, X.; Lin, L.; Zong, K.; Li, M.; Chen, H.; et al. Improved in Situ Hf Isotope Ratio Analysis of Zircon Using Newly Designed X Skimmer Cone and Jet Sample Cone in Combination with the Addition of Nitrogen by Laser Ablation Multiple Collector ICP-MS. *J. Anal. At. Spectrom.* **2012**, *27*, 1391–1399. [CrossRef]
47. Qiu, Z. *Geochemistry and Hf Isotopes of Zircon Megacrysts in Cenozoic Basalts Along Eastern China and Its Implications for Crust-Mantle Interaction Beneath Subcontinental Lithosphere Mantle*; Zhejiang University: Hangzhou, China, 2009.
48. Sun, S.-S.; McDonough, W.F. Chemical and Isotopic Systematics of Oceanic Basalts: Implications for Mantle Composition and Processes. *Geol. Soc.* **1989**, *42*, 313–345. [CrossRef]
49. Harley, S.L.; Kelly, N.M. Zircon Tiny but Timely. *Elements* **2007**, *3*, 13–18. [CrossRef]
50. Corfu, F.; Polteau, S.; Planke, S.; Faleide, J.I.; Svensen, H.; Zayoncheck, A.; Stolbov, N. U–Pb Geochronology of Cretaceous Magmatism on Svalbard and Franz Josef Land, Barents Sea Large Igneous Province. *Geol. Mag.* **2013**, *150*, 1127–1135. [CrossRef]
51. Zhu, Z.; Campbell, I.H.; Allen, C.M.; Brocks, J.J.; Chen, B. The Temporal Distribution of Earth's Supermountains and Their Potential Link to the Rise of Atmospheric Oxygen and Biological Evolution. *Earth Planet. Sci. Lett.* **2022**, *580*, 117391. [CrossRef]
52. Borghini, G.; Fumagalli, P.; Rampone, E. The Stability of Plagioclase in the Upper Mantle: Subsolidus Experiments on Fertile and Depleted Lherzolite. *J. Petrol.* **2010**, *51*, 229–254. [CrossRef]
53. Griffin, W.L.; Pearson, N.J.; Belousova, E.; Jackson, S.E.; van Achterbergh, E.; O'Reilly, S.Y.; Shee, S.R. The Hf Isotope Composition of Cratonic Mantle: LAM-MC-ICPMS Analysis of Zircon Megacrysts in Kimberlites. *Geochim. Cosmochim. Acta* **2000**, *64*, 133–147. [CrossRef]
54. Heaman, L.M.; Creaser, R.A.; Cookenboo, H.O.; Chacko, T. Multi-Stage Modification of the Northern Slave Mantle Lithosphere: Evidence from Zircon- and Diamond-Bearing Eclogite Xenoliths Entrained in Jericho Kimberlite, Canada. *J. Petrol.* **2006**, *47*, 821–858. [CrossRef]
55. Giuliani, A.; Phillips, D.; Woodhead, J.D.; Kamenetsky, V.S.; Fiorentini, M.L.; Maas, R.; Soltys, A.; Armstrong, R.A. Did Diamond-Bearing Orangeites Originate from MARID-Veined Peridotites in the Lithospheric Mantle? *Nat. Commun.* **2015**, *6*, 6837. [CrossRef]
56. Sun, J.; Tappe, S.; Kostrovitsky, S.I.; Liu, C.-Z.; Skuzovatov, S.Y.; Wu, F.-Y. Mantle Sources of Kimberlites through Time: A U-Pb and Lu-Hf Isotope Study of Zircon Megacrysts from the Siberian Diamond Fields. *Chem. Geol.* **2018**, *479*, 228–240. [CrossRef]
57. Boehnke, P.; Watson, E.B.; Trail, D.; Harrison, T.M.; Schmitt, A.K. Zircon Saturation Re-Revisited. *Chem. Geol.* **2013**, *351*, 324–334. [CrossRef]
58. Borisova, A.Y.; Bindeman, I.N.; Toplis, M.J.; Zagrtdenov, N.R.; Guignard, J.; Safonov, O.G.; Bychkov, A.Y.; Shcheka, S.; Melnik, O.E.; Marchelli, M.; et al. Zircon Survival in Shallow Asthenosphere and Deep Lithosphere. *Am. Mineral.* **2020**, *105*, 1662–1671. [CrossRef]
59. Garnier, V.; Ohnenstetter, D.; Giuliani, G.; Fallick, A.E.; Phan Trong, T.; Hoàng Quang, V.; Pham Van, L.; Schwarz, D. Basalt Petrology, Zircon Ages and Sapphire Genesis from Dak Nong, Southern Vietnam. *Mineral. Mag.* **2005**, *69*, 21–38. [CrossRef]
60. Hoskin, P.W.O.; Ireland, T.R. Rare Earth Element Chemistry of Zircon and Its Use as a Provenance Indicator. *Geology* **2000**, *28*, 627. [CrossRef]
61. Grimes, C.B.; John, B.E.; Kelemen, P.B.; Mazdab, F.K.; Wooden, J.L.; Cheadle, M.J.; Hanghøj, K.; Schwartz, J.J. Trace Element Chemistry of Zircons from Oceanic Crust: A Method for Distinguishing Detrital Zircon Provenance. *Geology* **2007**, *35*, 643. [CrossRef]
62. Campbell, L.S.; Compston, W.; Sircombe, K.N.; Wilkinson, C.C. Zircon from the East Orebody of the Bayan Obo Fe–Nb–REE Deposit, China, and SHRIMP Ages for Carbonatite-Related Magmatism and REE Mineralization Events. *Contrib. Miner. Pet.* **2014**, *168*, 1041. [CrossRef]
63. Saava, E.V.; Belyastsky, B.V.; Antonov, A.B. Carbonatitic Zircon-Myth or Reality: Mineralogical-Geochemical Analyses. Available online: http://alkaline09.narod.ru/abstracts/Savva_Belyatsky.Htm (accessed on 30 December 2018).
64. Foley, S.F.; Yaxley, G.M.; Rosenthal, A.; Buhre, S.; Kiseeva, E.S.; Rapp, R.P.; Jacob, D.E. The Composition of Near-Solidus Melts of Peridotite in the Presence of CO_2 and H_2O between 40 and 60 Kbar. *Lithos* **2009**, *112*, 274–283. [CrossRef]

65. Grimes, C.B.; Wooden, J.L.; Cheadle, M.J.; John, B.E. "Fingerprinting" Tectono-Magmatic Provenance Using Trace Elements in Igneous Zircon. *Contrib. Mineral. Petrol.* **2015**, *170*, 46. [CrossRef]
66. Turner, S.; Wilde, S.; Wörner, G.; Schaefer, B.; Lai, Y.-J. An Andesitic Source for Jack Hills Zircon Supports Onset of Plate Tectonics in the Hadean. *Nat. Commun.* **2020**, *11*, 1241. [CrossRef] [PubMed]
67. Xu, X.; O'Reilly, S.Y.; Griffin, W.L.; Zhou, X. Enrichment of Upper Mantle Peridotite: Petrological, Trace Element and Isotopic Evidence in Xenoliths from SE China. *Chem. Geol.* **2003**, *198*, 163–188. [CrossRef]
68. Xu, X.; O'Reilly, S.Y.; Griffin, W.L.; Zhou, X. Genesis of Young Lithospheric Mantle in Southeastern China: An LAM–ICPMS Trace Element Study. *J. Petrol.* **2000**, *41*, 111–148. [CrossRef]
69. Zhang, H.-F. Transformation of Lithospheric Mantle through Peridotite-Melt Reaction: A Case of Sino-Korean Craton. *Earth Planet. Sci. Lett.* **2005**, *237*, 768–780. [CrossRef]
70. Zheng, J.P.; Griffin, W.L.; O'Reilly, S.Y.; Yu, C.M.; Zhang, H.F.; Pearson, N.; Zhang, M. Mechanism and Timing of Lithospheric Modification and Replacement beneath the Eastern North China Craton: Peridotitic Xenoliths from the 100 Ma Fuxin Basalts and a Regional Synthesis. *Geochim. Cosmochim. Acta* **2007**, *71*, 5203–5225. [CrossRef]
71. Xu, W.; Hergt, J.M.; Gao, S.; Pei, F.; Wang, W.; Yang, D. Interaction of Adakitic Melt-Peridotite: Implications for the High-Mg # Signature of Mesozoic Adakitic Rocks in the Eastern North China Craton. *Earth Planet. Sci. Lett.* **2008**, *265*, 123–137. [CrossRef]
72. Tang, Y.-J.; Zhang, H.-F.; Ying, J.-F.; Su, B.-X. Widespread Refertilization of Cratonic and Circum-Cratonic Lithospheric Mantle. *Earth-Sci. Rev.* **2013**, *118*, 45–68. [CrossRef]
73. Lin, A.-B.; Zheng, J.-P.; Xiong, Q.; Aulbach, S.; Lu, J.-G.; Pan, S.-K.; Dai, H.-K.; Zhang, H. A Refined Model for Lithosphere Evolution beneath the Decratonized Northeastern North China Craton. *Contrib. Miner. Pet.* **2019**, *174*, 15. [CrossRef]
74. Zhou, Q.; Wu, F.Y.; Yang, Y.H.; Sun, D.Y.; Ge, W.C. Sr-Nd-Hf-Os Isotopic Characterizations of the Jiaohe Peridotite Xenoliths in Jilin Province and Constraints on the Lithospheric Mantle Age in Northeastern China. *Acta Petrol. Sin.* **2007**, *23*, 1269–1280. (In Chinese with English Abstract)
75. Yu, S.-Y.; Xu, Y.-G.; Huang, X.-L.; Ma, J.-L.; Ge, W.-C.; Zhang, H.-H.; Qin, X.-F. Hf–Nd Isotopic Decoupling in Continental Mantle Lithosphere beneath Northeast China: Effects of Pervasive Mantle Metasomatism. *J. Asian Earth Sci.* **2009**, *35*, 554–570. [CrossRef]
76. Niu, Y. Generation and Evolution of Basaltic Magmas: Some Basic Concepts and a Hypothesis for the Origin of the Mesozoic-Cenozoic Volcanism in Eastern China. *Geol. J. China Univ.* **2005**, *11*, 9–46.
77. Huang, J.; Zhao, D. High-Resolution Mantle Tomography of China and Surrounding Regions. *J. Geophys. Res.* **2006**, *111*, B09305. [CrossRef]
78. Xu, Y.; Li, H.; Hong, L.; Ma, L.; Ma, Q.; Sun, M. Generation of Cenozoic Intraplate Basalts in the Big Mantle Wedge under Eastern Asia. *Sci. China Earth Sci.* **2018**, *61*, 869–886. [CrossRef]
79. Lin, J.; Xu, Y.; Sun, Z.; Zhou, Z. Mantle Upwelling beneath the South China Sea and Links to Surrounding Subduction Systems. *Natl. Sci. Rev.* **2019**, *6*, 877–881. [CrossRef] [PubMed]

Disclaimer/Publisher's Note: The statements, opinions and data contained in all publications are solely those of the individual author(s) and contributor(s) and not of MDPI and/or the editor(s). MDPI and/or the editor(s) disclaim responsibility for any injury to people or property resulting from any ideas, methods, instructions or products referred to in the content.